Journal of Colloid and Interface Science 369 (2012) 256–266

Contents lists available at SciVerse ScienceDirect

Journal of Colloid and Interface Science

www.elsevier.com/locate/jcis

The *cis*-bis(decanoate)tin phthalocyanine/DPPC film at the air/water interface

Salvador Ramos [a], Cristina Garza [a], Hiram I. Beltran [b], José Campos-Terán [c], Jesús Arenas-Alatorre [a], Rolando Castillo [a,*]

[a] Instituto de Física, Universidad Nacional Autónoma de Mexico, P.O. Box 20-364, Mexico DF 01000, Mexico
[b] Departamento de Ciencias Naturales, DCNI, Universidad Autónoma Metropolitana, Unidad Cuajimalpa, Artificios 40, Mexico DF 01120, Mexico
[c] Departamento de Procesos y Tecnología, DCNI, Universidad Autónoma Metropolitana, Unidad Cuajimalpa, Artificios 40, Mexico DF 01120, Mexico

ARTICLE INFO

Article history:
Received 13 September 2011
Accepted 26 November 2011
Available online 7 December 2011

Keywords:
Tin phthalocyanine
Phthalocyanine/DPPC films
Air/water interface films
Tin phthalocyanines/DPPC mixtures
cis-Bis-decanoate-tin^{IV} phthalocyanine

ABSTRACT

Films made of *cis*-bis-decanoate-tin^{IV} phthalocyanine (PcSn10) and racemic dipalmitoylphosphatidylcholine (DPPC) are studied with compression isotherms and Brewster angle microscopy (BAM) at the air/water interface. Films enriched in PcSn10 present phase separation elliptical-shaped domains. These domains present optical anisotropy and molecular order. They are enriched in PcSn10, and the film outside these domains is enriched in DPPC, as shown in by high-angle annular dark-field transmission electron microscopy on Langmuir–Blodgett (LB) transferred films. Film collapse area and atomic force microscopy images of LB transferred films on mica indicate that the films are actually multilayers. A computational survey was performed to determine how the PcSn10 molecules prefer to self-assemble, in films basically made of PcSn10. The relative energetic stability for several dimeric assemblies was obtained, and a crystal model of the film was developed through packing and repeating the PcSn10 molecules, along the crystallographic directions of the unit cell. Our results contribute to understanding the strong interaction between PcSn10 and DPPC at the air/water interface, where even small quantities of DPPC (~1–2%) can modify the film in an important way.

1. Introduction

Since the time of its discovery, the phthalocyanine (Pc) macrocycle has been the subject of extensive studies, mainly devoted to clarifying its size, chemical and electronic structure, and designable properties [1]. In addition, this type of molecule is synthetically susceptible to many chemical modifications to provide peculiar, innovative, and advantageous characteristics to the Pc backbone. A wide range of strategies have been reported for modifying the supramolecular architecture of this backbone with long side linear or branched alkyl, alkoxymethyl, or alkoxy chains [1]. In the same way, there is an important effort to obtain Pc molecules with a variety of different atoms and ligands attached into the central cavity of the macrocycle [2,3]. Substitution of the central atom gives the opportunity of modifying molecular properties without chemically changing the Pc skeleton. Metal–Pc (MPc) with a single metal atom in the center can be classified in planar and in nonplanar architectures. In the case of nonplanar MPc, the central metal atom is often too large to completely fit into the cavity; therefore, it sticks out of the molecular plane and a bending of the Pc skeleton in the opposite direction occurs to relax the structure and minimize hindrance. Electronic, photonic, and magnetic properties of phthalocyanines, as well as their metal complex derivatives, have been thoroughly investigated because of their high stability, the presence of intense π–π^* transitions in the visible region, and their redox activity [1,2]. Baker et al. [4] first demonstrated that Pc molecules can be deposited in LB multilayers. Since then, incorporation of Pc structures as the main component in organic thin films and the investigation of the resulting properties are objectives of extensive research [5–10]. In particular, great efforts have been made toward the aim of immobilizing individual molecules on a solid substrate, with minimal impact on the chemical and physical properties of the adsorbed molecules, to reach both the goal of high-resolution structural characterization [9,11–13], and the development of potential applications [14–17]. One way of structural characterization on solid substrates, after Langmuir–Blodgett (LB) deposition, is using a surface probe microscopy (SPM) to identify molecular arrangement.

Photodynamic therapy of cancer is a noninvasive treatment of small and superficial tumors. The therapy is based on the systemic administration of a tumor-localizing photosensitizer followed by illumination with light of appropriate wavelength. The resulting photodynamic reactions give rise to singlet oxygen and to other oxygen active molecules, acting as cytotoxic species, leading to tumor necrosis and its destruction. Among the more promising second-generation photosensitizers are phthalocyanines [18–21]. Unfortunately, photosensitizers like phthalocyanines are generally insoluble in

* Corresponding author. Fax: +52 55 561 61535.
E-mail address: rolandoc@fisica.unam.mx (R. Castillo).

0021-9797/$ - see front matter © 2011 Elsevier Inc. All rights reserved.
doi:10.1016/j.jcis.2011.11.072

water or biologically compatible solvents. They must be administered *in vivo* by means of delivery systems, like phospholipid liposomes, where the interaction of photosensitizers with the phospholipid liposome bilayer seems to be a key issue to novel procedures [21]. With this motivation, the aim of this paper is to study the behavior of films at the air/water (W) made of a MPc derivative (*cis*-bis-decanoate-tin^{IV} phthalocyanine, PcSn10), with a metal atom with two decanoate tails attached (see Fig. 1) that provides an enhanced solubility to the MPc molecule in organic solvents, and a phospholipid (racemic dipalmitoylphosphatidylcholine, DPPC) that is an important component in formulations for the preparation of liposomes. As far as we know, this binary system has not been studied before. This film can be a model of one leaflet of the liposome bilayer, particularly at high concentrations of DPPC. This is a first step to determine how PcSn10 and DPPC interact in a film, prior to determine the effect of adding PcSn10 on actual liposomes, which are a mixture of phospholipids appropriate to for the administration of the PcSn10.

2. Experimental section

2.1. Reagents

$PcSn^{IV}Cl_2$ was allowed to react with the potassium salt of decanoic acid in a 1:2 M ratio in dimethylformamide and exposed to microwave irradiation (power 300–600 W at 150 °C) for 10 min, to produce *cis*-bis-decanoate-tin^{IV} phthalocyanine ($PcSn(O_2C(CH_2)_8CH_3)_2$ or PcSn10) [22,23]. This compound was separated using methanol/water solvent mixtures on the reaction crude producing a metallic blue powder in a yield of 76%. Purity was determined using ^{1}H NMR, which was ca. 99%. However, a further purification was carried out: 0.5 g of PcSn10 was dissolved in 20 mL of HPLC grade chloroform. This solution was applied into a preparative alumina plate and eluted with HPLC grade chloroform. After a Soxlet extraction of the eluted fraction, and evaporation under reduced pressure, a purified compound was produced. Racemic dipalmitoylphosphatidylcholine (DPPC) ⩾ 99% was obtained from Sigma–Aldrich Chemie (Switzerland).

2.2. UV–visible spectra

UV–visible measurements made on PcSn10/DPPC chloroform solutions were carried out through scans from 190 to 1100 nm (bandwidth 0.5 nm) in absorbance mode using an Evolution 300 UV–visible spectrophotometer from Thermoscientific (Thermo Fisher Scientific, Inc., Ma). Spectra were recorded by using the vision Pro Thermo Electron UV–visible spectrometry software version 4.10.

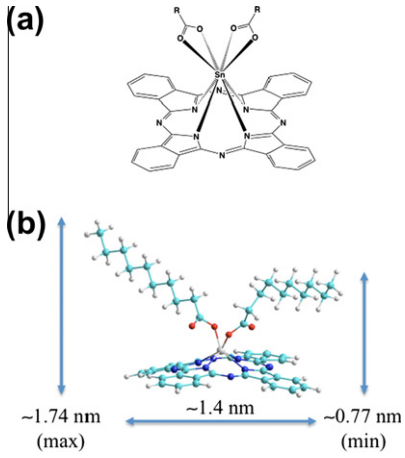

Fig. 1. *Cis*-bis-decanoate-tin^{IV} phthalocyanine (PcSn10): (a) scheme where R are decanoate tails and (b) approximate molecular size.

2.3. Monolayers at the air/water interface

DPPC, PcSn10, and their mixtures were spread onto a subphase of ultrapure water (Barnsteed, USA; Nanopure-UV, 18.2 MΩ) in a Langmuir trough. When needed, the subphase pH was modified, depending on the case with H_2SO_4 of 95–97% (Merck, Germany), with NaOH ⩾ 98% (Sigma–Aldrich, MO), or using a phosphate buffer solution: sodium phosphate monobasic ⩾99% and sodium phosphate dibasic ⩾99% (both from Sigma–Aldrich MO). Spreading solutions were made with HPLC grade chloroform ⩾99.8% (Sigma–Aldrich, USA). The spreading solution concentration to prepare the DPPC monolayer was of ~1.00 mg/mL. For the case of mixtures, the concentration of the spreading solution was between 0.32 and 2.5 mg/mL, in both PcSn10 + DPPC; the amount of PcSn10 was kept constant =0.25 mg/mL. After 15 min of deposition for allowing solvent evaporation, trough barriers were closed at a speed of ~7–8 cm^2/min.

2.4. Langmuir troughs

Two Nima LB troughs (Nima Technology Ltd., England) were used. Model 601 BAM was used to make compression isotherms and BAM observations, and model TKB 2410A for developing LB films. In both cases, a Wilhelmy plate was used to measure the surface pressure, $\Pi(A,T) = \gamma_o - \gamma$, which is the surface tension difference between the uncovered and the covered subphase; T is temperature and A is area per molecule. Both troughs were isolated from vibrations. Temperature was kept constant with the aid of a water circulator bath (Cole-Parmer 1268-24, USA). All experiments were carried out in a clean-room laboratory.

2.5. Brewster angle microscopy (BAM)

[24,25]. During compression, monolayers were observed using an Elli2000 imaging ellipsometer (Nanofilm Technologie GmbH, Germany) in the BAM mode (spatial resolution of ~2 and ~1 μm using the 10× and 20× objectives, respectively). BAM observations of the films at the air/water interface (BAM1-plus instrument (Nanofilm Technologie GmbH, Germany with a spatial resolution of ~4 μm) were performed during the development of the LB films to assure that the film at the air–water interface was of the best quality to produce a LB film.

2.6. Atomic force microscopy (AFM)

LB transferred monolayers (Π = 4 mN/m and at a rising up speed of 3 mm/min) on freshly cleaved mica were scanned with a scanning probe microscope (JSTM-4200 JEOL, Japan) with a 25 μm × 25 μm scanner at high vacuum (10^{-4} Pa). Non-contact silicon cantilevers were used with a nominal force constant of 40 N/m (NSC/AlB5, Mickomash, OR) made of highly doped Si with back side coating of Al (measured Q-factor ~1000 in air).

Topographic and phase images were obtained by using the dynamic mode (AC mode), where the cantilever is externally oscillated close to its fundamental resonance. It was operated using amplitude modulation [26] (AM) and frequency modulation [27] (FM). In AM, changes in the oscillation amplitude of the cantilever, or phase lag of the cantilever oscillation relative to the signal sent to the cantilever's piezo-driver, provide the feedback signal for imaging, i.e., a z-scanner controller moves the sample along the vertical direction such that the oscillation amplitude and phase of the vibrating cantilever stays at a fixed value (intermittent contact or tapping mode). FM relies on detecting small changes in the cantilever resonant frequency, which occur in response to the tip–

sample interaction [27]. These frequency shifts, keeping the resonant frequency at constant amplitude, can then be used as a feedback signal for imaging. Force sensitivity is enhanced by using high vacuum, because it increases the mechanical cantilever Q-factor. The FM method does not suffer from the long relaxation times of amplitude variation in the AM method, producing in general images with a better resolution. Also, it allows distinguishing between the attractive and repulsive force regimes depending on the sign of the frequency shift [27].

2.7. Transmission electron microscopy (TEM)

Films of the DPPC/PcSn10 were LB transferred on collodion-coated Cu grids for TEM. Microstructural analysis of these transferred films was performed in a TEM JEM-2010F FASTEM (JEOL, Japan) with an ultimate resolution point to point of 1.9 Å fitted with a Gatan Image Filter. Conventional TEM, as well as high-angle annular dark-field (HAADF) [28,29] modes, was employed in the analysis. The latter is highly sensitive to variations in the atomic number of atoms in the sample; this enables us to obtain *Z*-contrast images of the film sample. In the HAADF TEM micrographs, bright areas are enriched in the heavy metal (tin) and dark areas are depleted in that heavy metal.

2.8. Semiempirical calculations

To understand how PcSn10 molecules prefer to self-assemble in films made essentially of these molecules, a computational study to determine the most stable chemical structure of dimeric assemblies of PcSn10 was carried out by using the Hyperchem (release 8) program. The algorithms are based on the parameterized model number 3 (PM3) method, which is a semiempirical method for quantum calculation of molecular electronic structure that is based on the neglect of differential diatomic overlap (NDO) integral approximation [30–32]. This method was selected because the size of the ensemble units of PcSn10 to be studied is substantial, and it is more practical to use it than more refined and expensive procedures, as those based on density functional theory or *ab initio* calculations. In addition, the PM3 method has parameters to calculate tin atoms, and the resulting structures can resemble quite well experimentally observed structural features. Namely, the anisobidentate coordination modes of the carboxylic moieties surrounding the tin atom in PcSn10 are well reproduced, when they are compared with calculated gas phase and X-ray structures [22,23]. Unfortunately, it is not possible to perform geometric or energetic comparisons for PcSn10 ensembles with the Austin model 1 (AM1) method, because the tin atom is not parameterized. Therefore, a full set of PM3 calculations was performed to determine the geometry of several dimeric assembly units to determine the most stable one. The initial coordinates of the ensemble units were extracted from the PcSn10 crystallographic coordinates at the Cambridge Structural Database (CSD) [33,34]. An important number of optimizations were carried out to get the geometry and energy of the dimeric assembly units with a coarse convergence criteria of <0.4 kcal/mol Å. For a better convergence level, e.g., <0.1 kcal/mol Å, the calculation required much more computational cycles (more than 10,000), and in some cases, this convergence limit could not be reached; hence, the coarser criteria was used.

3. Results

3.1. Isotherms and BAM observations for films of mixtures made of PcSn10 and DPPC

Fig. 2 presents the compression isotherms of films made with different proportions of PcSn10 and DPPC, ranging from pure PcSn10 to pure DPPC, at $T = 22.3$ °C. Six features are clearly observed: (A) At very low densities, all films present a phase that behaves in a similar way to the gas phase found in Langmuir monolayers; surface pressure is negligible at those densities. (B) When the film is rich in DPPC, it can undergo high surface pressures ($\Pi > 50$ mN/m) and presents an apparent film collapse at $\Pi \geqslant 57$ mN/m. When the PcSn10 concentration is larger than $X_{PcSn10} \sim 0.50$, the apparent collapse pressure drops down and it can reach values around $\Pi = 20$ mN/m. (C) The first-order phase transition of the monolayer corresponding to pure DPPC (~8 mN/m) fades away as the PcSn10 concentration increases in the film. The isothermal compression of pure DPPC monolayer typically produces a sequence of 2D phases proceeding with increasing surface density from gas (*G*), to liquid-expanded (*LE*), to tilted condensed (*TC*) [36]. In Fig. 2, a typical well-known BAM image for the DPPC monolayer at the LE/TC phase transition is presented. At the end of the compression, just the collapse is found. The large size of the hydrophilic head prevents a vertical tail arrangement. As a consequence, the untilted condensed phase (*UC*) does not exist in the DPPC monolayer [36–38]. (D) The film of pure PcSn10 is highly incompressible, reminiscent of a crystalline film. A typical BAM image of a film of pure PcSn10 is presented in Fig. 2. This film usually presents domains with irregular shapes that cannot properly heal as compression proceeds; some of them present many defects and look like spotted and other domains are very homogeneous. (E) As the pure DPPC monolayer is isothermally compressed, the gas phase ends up at $A \sim 105$ Å^2/molec; in contrast, pure PcSn10 gas phase ends up at $A \sim 80$ Å^2/molec. Collapse is found in pure DPPC and in pure PcSn10 at surface areas of ~43–45 Å^2/molec and of ~70–72 Å^2/molec, respectively. Given the spatial dimensions of PcSn10 according to the sizes given in Fig. 1b, the collapse should be roughly at 176 Å^2/molec (averaging the vertical length) when the molecule would be laying edge-on over the interface. Therefore, the PcSn10 film at the air/water interface seems to be a multilayer formed of well-packed molecules, probably leaning sideways onto the air/water interface, and stabilized thanks to the degrees of freedom provided by the two tails attached to the

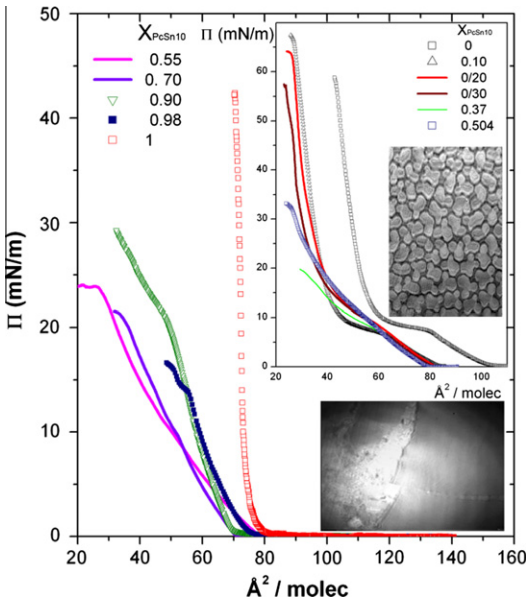

Fig. 2. Isotherms of films made of PcSn10 and DPPC at different PcSn10 mol fractions, X_{PcSn10}, as indicated in the legend. BAM images for the single-component films are included, upper image: DPPC ($\Pi = 10.7$ mN/m, full width 452 μm); lower image: PcSn10 ($\Pi = 27$ mN/m, full width 657 μm). Isotherms are in a range of ~0.4 °C around $T = 22.3$ °C, and at pH = 5.6–5.8.

tin atom. Except for the case of films highly enriched in PcSn10, all mixtures between the pure components present an apparent collapse at very low areas ~25–30 Å^2/molec, which is close to a half of the collapse area of the films using the pure components. Therefore, apparently these films are not made of a single molecular layer, indicating that at the air/water interface there exist a complicated self-assembly, where assembled structures seem to vary with concentration. (E) Isotherms were made at least in triplicates and in general the curves overlap; they are quite reproducible. Kinks where pressure deviates from zero fluctuate in the range of 2–3 Å/molec, and as it is common in films at the air/water interface, collapse pressure fluctuates. Compression expansion cycles were also done and the curves essentially overlap.

To obtain information about how DPPC affects PcSn10 in solution, before spreading on the air/water interface to form the film, we performed UV–visible measurements in mixtures of DPPC and PcSn10 at different concentrations, all in chloroform solution. The location and shape of the Q-band (at ~680 nm) can be used to estimate the aggregation behavior of MPc [35]. In Fig. 3, the UV–visible spectrum of pure PcSn10 at 0.05 mg/mL presents a narrow absorption band at 680 nm. In contrast, the UV–visible spectrum for pure PcSn10 at 0.2 mg/mL presents a broader absorption band at 680 nm, which is evidence of a small aggregation stage. When the DPPC/PcSn10 chloroform solutions were prepared in concentrations close to that used for the spreading solution (0.25 mg/mL in PcSn10), it was observed that no matter the relative amount of DPPC added to the mixture (PcSn10/DPPC = 10/90–90/10 in w% for a fixed concentration of PcSn10 = 0.25 mg/mL; see Fig. 3), the resulting spectra present broad absorption bands located between 630 and 720 nm. This indicates that in the DPPC/PcSn10 solutions, the DPPC molecules do not prevent the formation of small clusters of PcSn10 molecules, even when the DPPC concentration is high. Therefore, the DPPC/PcSn10/chloroform spreading solution is not spreading just single molecules at the air/water interface, but small aggregates of PcSn10, accompanied with varying amounts of DPPC depending on the relative concentration of the components in the spreading solution. Probably, these aggregates will tend to reorganize at the air/water interface, because there are different interactions that will come into play there in addition to the tendency of PcSn10 molecules to interact among them, as the tendency to avoid the water subphase, and the hydrophobic interaction with both the DPPC tail and air. Since the size of the aggregates is below the

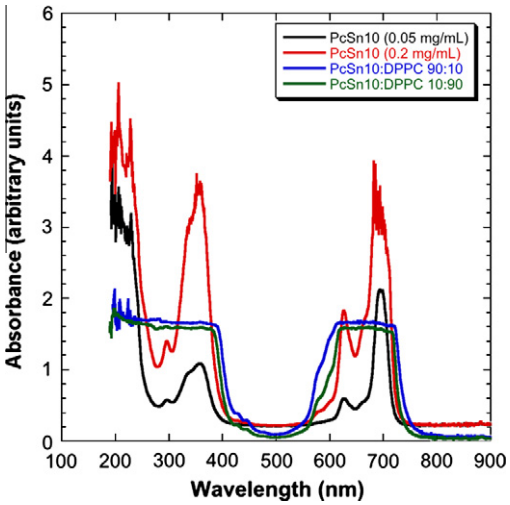

Fig. 3. UV–visible spectra of chloroform solutions of pure $PcSn10_2$ and of mixtures of PcSn10 and DPPC at ratios of 10/90 and 90/10 in w%, with a constant concentration of PcSn10 = 0.25 mg/mL).

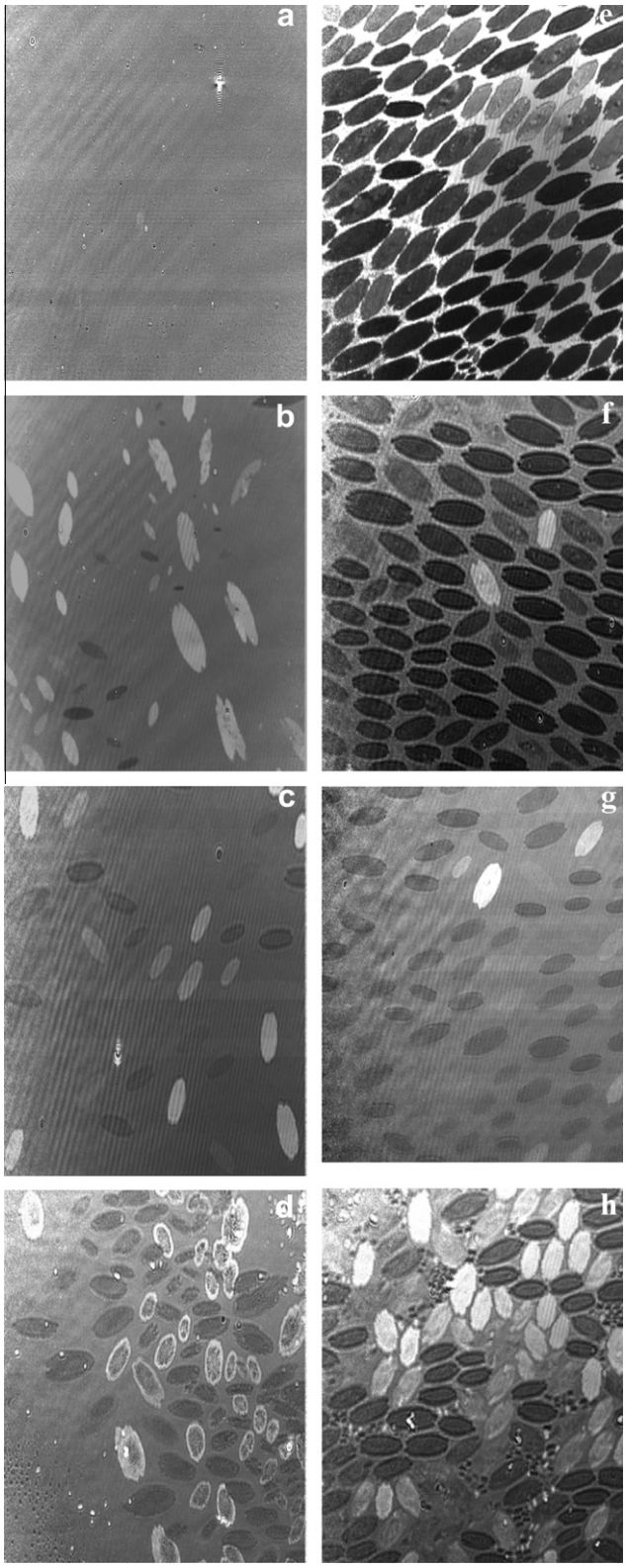

Fig. 4. BAM images of the PcSn10/DPPC films. (a) Typical image for mixtures with $X_{PcSn10} \leqslant 0.7$ where just one kind of shade is observed; in this particular case $X_{PcSn10} = 0.7$, $T = 22.5$ °C, $\Pi = 27.2$ mN/m. Typical images for mixtures with $X_{PcSn10} \geqslant 0.7$: (b) $X_{PcSn10} = 0.78$, $T = 22.4$ °C, $\Pi = 11.7$ mN/m. (c) $X_{PcSn10} = 0.87$, $T = 23.4$ °C, $\Pi = 3.0$ mN/m. (d) $X_{PcSn10} = 0.98$, $T = 22.0$ °C, $\Pi = 0.2$ mN/m. (e) $X_{PcSn10} = 0.87$, $T = 22.9$ °C, $\Pi = 27.0$ mN/m. (f) $X_{PcSn10} = 0.87$, $T = 22.0$ °C, $\Pi = 22.3$ mN/m. (g) $X_{PcSn10} = 0.87$, $T = 22.6$ °C, $\Pi = 3.8$ mN/m. (h) $X_{PcSn10} = 0.98$, $T = 22.0$ °C, $\Pi = 11.7$ mN/m. In all the cases pH = 5.6–5.8. The horizontal full width is 461 μm for each individual image.

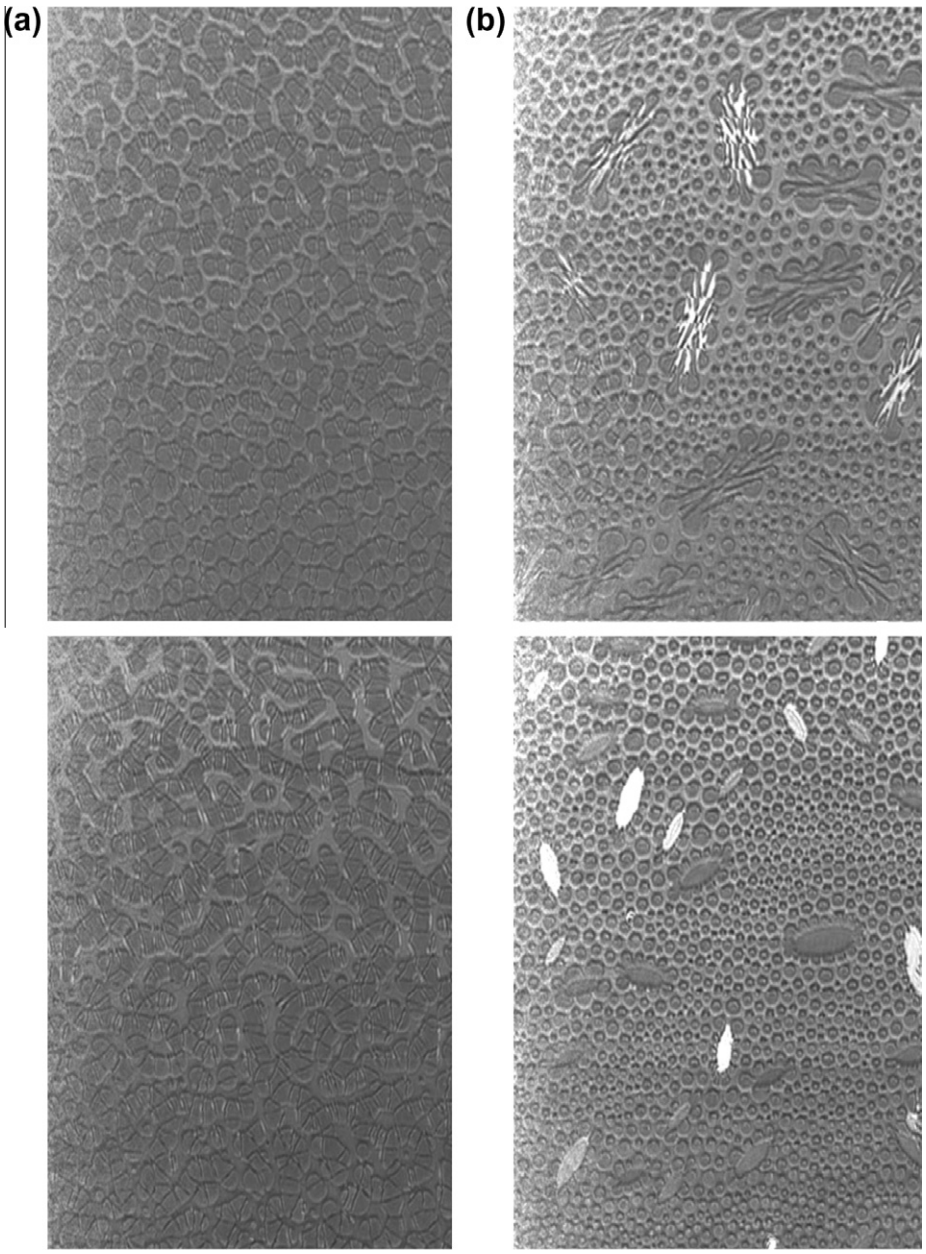

Fig. 5. Formation of the elliptical-shaped domains at $X_{PcSn10} = 0.87$. Images of the film: (a) $\Pi \sim 0$ mN/m, both images correspond to $A = 127$ Å^2/molec. (b) $\Pi \sim 0$ mN/m, upper panel corresponds to $A = 112$ Å^2/molec, and lower panel corresponds to $A = 100$ Å^2/molec, $T = 23.3$ °C, pH = 5.6–5.8. The horizontal full width is 461 μm for each individual image.

BAM resolution limit, it is not clear whether these aggregates are homogeneously distributed in the film at the air/water interface or they are actually molecularly dispersed.

BAM images of the film at the air/water interface are not particularly illuminating when $X_{PcSn10} \leqslant 0.70$. At those concentrations, BAM observations reveal a homogeneous film that most of the times show just one kind of shade (light gray, Fig. 4a). In the limit of resolution of this technique (~2 and ~1 μm), there are no domains revealing segregation or some kind of molecular order, which could give origin to different textures, i.e., the films look like condensed disordered isotropic phases. In a few cases, it is possible to observe irregular bands of slight different shade of gray crossing all the field of view. In contrast, when $X_{PcSn10} > 0.7$, domains of elliptical shape appear as the film is compressed, revealing some kind of phase separation. These elliptical-shaped domains have a different hue of gray depending on their orientation with respect to the polarized light of the Brewster angle microscope, revealing that the domains present optical anisotropy, surely as a consequence of a specific molecular order, which is different to the material outside these domains. In Fig. 4b–h, we present some examples of these domains that recall coexisting phases in Langmuir monolayers. These images correspond to the compression of different films at almost the same temperature, so the images can be compared. Figs. 4a–d present film images at different surface pressures when the PcSn10 concentration increases from $X_{PcSn10} = 0.70$ to $X_{PcSn10} = 0.98$. For $X_{PcSn10} > 0.7$, as the film is more concentrated in PcSn10, lower surface pressures are needed to have roughly the same number of elliptical-shaped domains in the field of view. Figs. 4e–g present films with the same PcSn10 concentration ($X_{PcSn10} = 0.87$), but at different surface pressures (e: $\Pi = 27.0$ mN/m. f: $\Pi = 22.3$ mN/m. g: $\Pi = 3.8$ mN/m); as Π increases, the number of elliptical-shaped domains also increases;

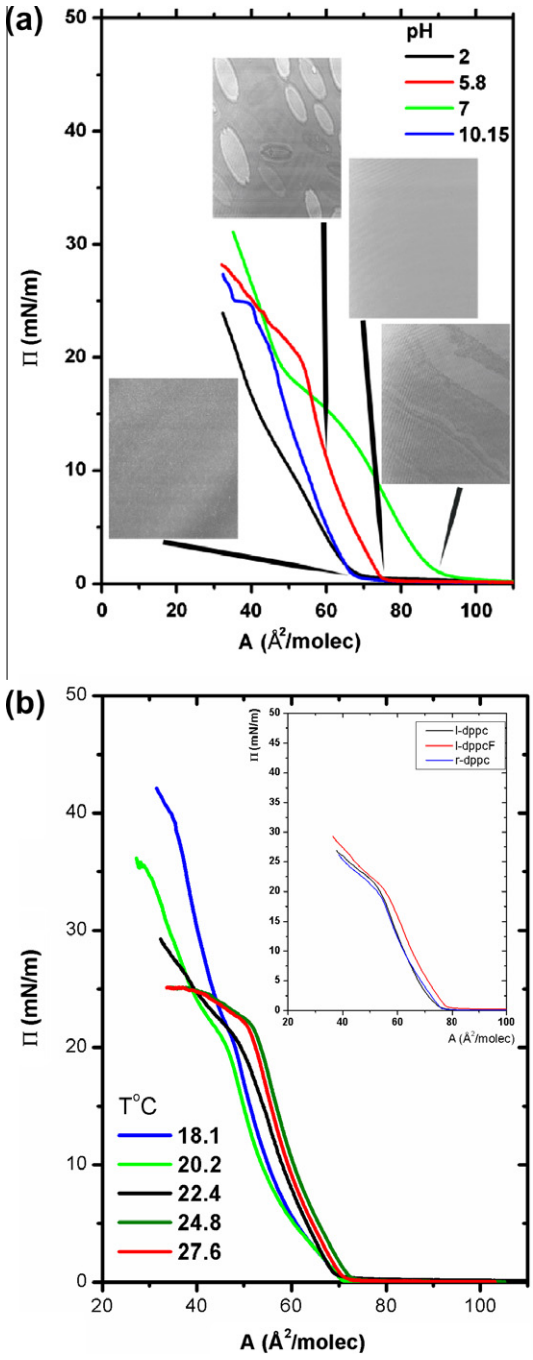

Fig. 6. (a) Compression isotherms as a function of pH for $X_{PcSn10} = 0.87$ at 22.7 °C (all isotherm temperatures are in a range of 0.7 °C from this value); BAM images correspond to $\Pi = 1.5$ mN/m (pH = 7), 0.2 mN/m (pH = 10.5), 0.3 mN/m (pH = 2), and 9.5 mN/m (pH = 5.8); the horizontal full width is 461 μm for each individual image. (b) Compression isotherms as a function of temperature for $X_{PcSn10} = 0.8$ at pH = 5.6–5.8. *Inset*: Isotherms where racemic DPPC is changed with *l*-DPPC and l-DPPCF. $T = 22.5$ °C.

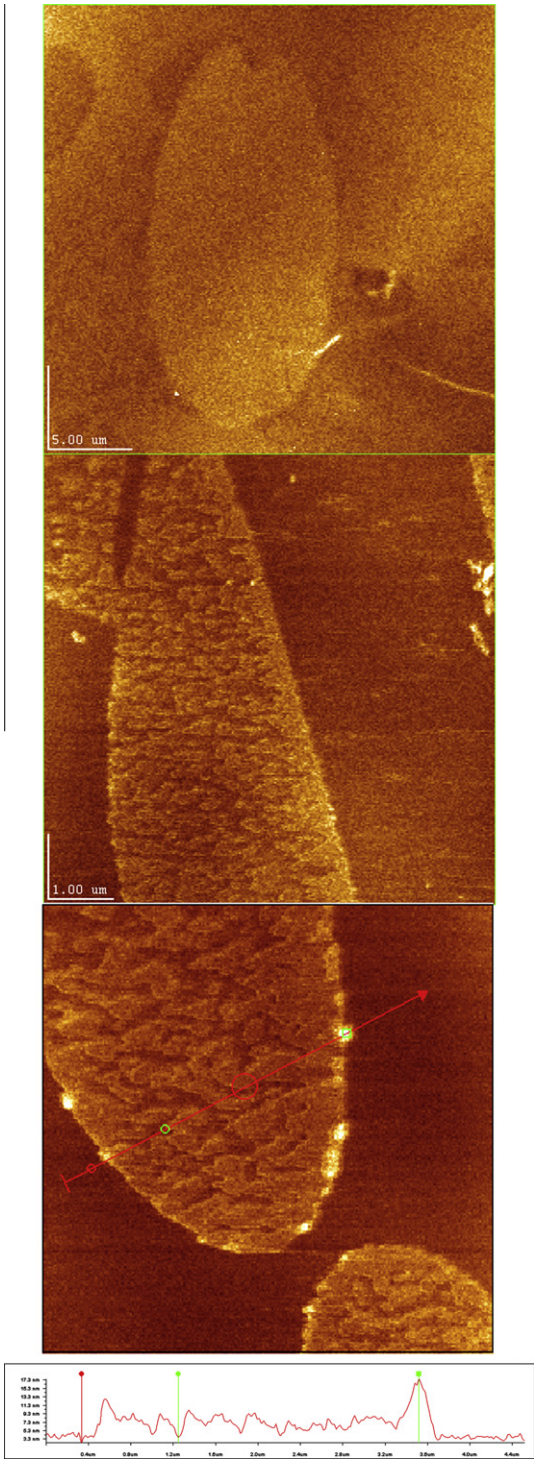

Fig. 7. Intermittent contact AFM topographic images of a phase separation elliptical-shaped domain in a Langmuir–Blodgett film made of PcSn10/DPPC over mica ($X_{PcSn10} = 0.87$ and pH = 5.6–5.8). Upper panel: a typical elliptical-shaped domain with a long axis ~24.2 μm and a short axis ~11.5 μm. Medium panel: a smaller domain with a short axis ~3.4 μm. Lower panel: amplification of the lower part of the domain presented in the medium panel with topographic measurements over the red line presented below: green markers: horizontal distance 2.27 μm, height difference 13.8 nm. Red markers: one at the left of the figure and the other just below the green marker to the right (on the peak), horizontal distance 3.18 μm, height difference 15.1 nm. (For interpretation of the references to color in this figure legend, the reader is referred to the web version of this article.)

and usually their size also increases. We observe the increase in the number and size of the domains as the PcSn10 concentration increases in Fig. 4b and h, which are at the same, $\Pi = 11.7$ mN/m, but at different concentration (b: $X_{PcSn10} = 0.78$. h: $X_{PcSn10} = 0.98$). The reflectivity of elliptic domains is not completely homogeneous. It is not strange to observe the rim of these domains very brilliant (Fig. 4d), revealing that the height of these domains is not uniform, although the rim also presents the same kind of optical anisotropy as the domains. In Fig. 4g, we observe a typical film close to the surface pressure where the LB films will be developed, as discussed below. It is important to note when the analyzer of the Brewster angle microscope is rotated, the domains change their hue of gray.

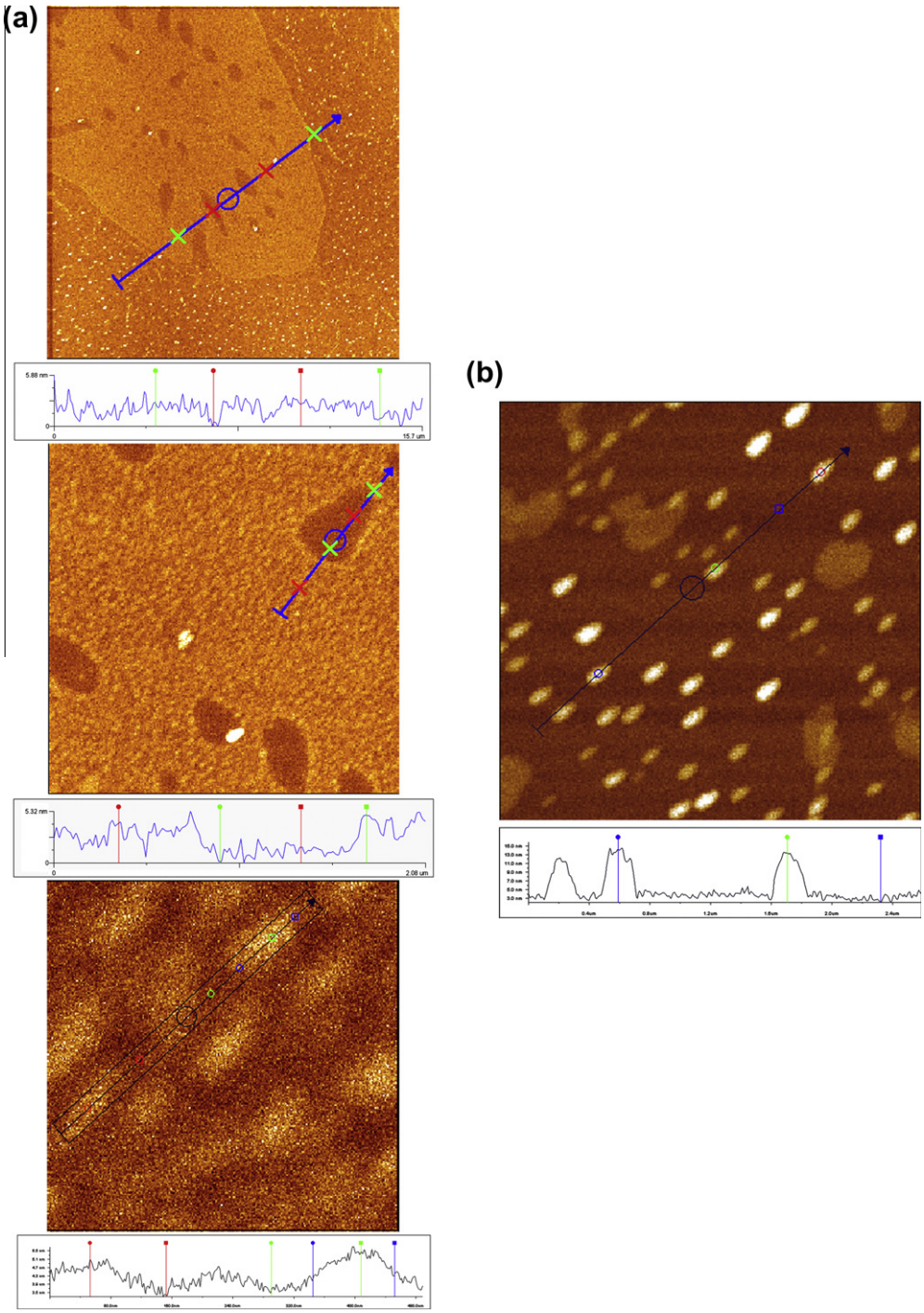

Fig. 8. Topographic images in a Langmuir–Blodgett film made of PcSn10/DPPC over mica showing an elliptical-shaped domain and its surroundings, using the DFM method. (a) Upper panel: over the blue line of 15.7 μm in length, red markers: horizontal distance 3.75 μm, height difference 2.2 nm. Green markers: horizontal distance 9.59 μm, height difference 1.6 nm. Medium panel: amplification of the previous image; over the blue line of 2.08 μm in length; red markers: horizontal distance 1.03 μm, height difference 2.5 nm. Green markers: horizontal distance 0.83 μm, height difference 4.7 nm. Lower panel: amplification of the previous image, average over sections of the indicated bar of ∼ 0.48 μm in length, red markers: horizontal distance 99.6 nm, height difference 1.78 nm. Blue markers: horizontal distance 107.3 nm, height difference 0.18 nm. Green markers: horizontal length 117.8 nm, height difference 1.84 nm. (b) Film outside the domain: over the blue line (∼3.0 μm in length) with grains with a major axis of ∼200 nm, red markers: horizontal distance 0.392 μm, height difference 13.8 nm. Blue markers: horizontal distance 1.73 μm, height difference 12.0 nm. Green markers: horizontal distance 0.614 μm, height difference 11.1 nm. (For interpretation of the references to color in this figure legend, the reader is referred to the web version of this article.)

We were able to capture how the elliptical-shaped domains are formed along the compression for the case of $X_{PcSn10} = 0.87$ (Fig. 5). The domain formation occurred when the film was compressed at vanishing surface pressures. After the waiting time that follows the deposition of the mixture at the air/water interface, the compression of the film started at very low area densities (∼127 Å^2/molec, $T = 23.3$ °C, pH = 5.6–5.8). Here, some kind of network joining elongated irregular structures is formed (Fig. 5a). These structures grow as compression is underway, forming a film similar to a carpet (light gray) with holes (dark gray). As compression goes on, some

of the holes cluster together, and inside the clusters, new irregular and elongated structures are formed (Fig. 5b). These structures have a different hue of gray (Fig. 4b, at 112 Å^2/molec) depending on their orientation with respect to the polarized light of the Brewster angle microscope. Therefore, they are optically anisotropic, revealing that there is a solid-like order. If the optically anisotropic film does not have a vertical axis z of symmetry, the reflected light is a function of the orientation of the film in its plane. As compression is taking place, still at vanishing surface pressures, the holes reduce their size below our limit of resolution, and small elliptical-shaped domains are formed from the irregular structures (Fig. 5b, at 100 Å^2/molec).

In Fig. 6, we present how the film is modified by pH and temperature as well as when the DPPC molecule is slightly modified. In Fig. 6a, we present compression isotherms as a function of pH, at $X_{PcSn10} = 0.87$ and $T = 22.7$ °C. As we observe, isotherms are substantially modified when pH is varied. Isotherms collapse at relatively low Π; the collapse is at a $\Pi \sim 25$–30 mN/m at pH $\sim$ 5.8. In addition, around pH $\sim$ 5.8, elliptical-shaped domains are observed with the aid of BAM at nonzero surface pressures, which are reminiscent of a phase separation. For very low surface pressures, see Figs. 4c and 5. This is why most of the isotherms reported here were developed at this pH. The DPPC charge has to be playing a role to produce these elliptical-shaped domains, since the DPPC isoelectric point is at pH $\sim$ 4 [39]. Here, DPPC molecules must be neutral or slightly negative. In Fig. 6b, we present how temperature affects the compression isotherms at $X_{PcSn10} = 0.87$ (pH = 5.6–5.8). As we can observe, collapse decreases as temperature is increased. In the inset of Fig. 6b, we have included isotherms where racemic DPPC was changed by *l*-DPPC and by fluorinated *l*-DPPCF. In the latter, one fluorine atom in the *l*-DPPC molecule is exchanged by one of the hydrogen atoms at the terminal methyl group. In general, the compression isotherms, as well as BAM images, hardly notice these changes. We observed that the exchange of one hydrogen with one fluorine atom at the terminal methyl group, which is a small hydrophobic change in the tail, translates upwards ($\Delta\Pi \sim 3$–4 mN m) the *LE*/*TC* transition of racemic DPPC at low temperatures; this difference fades away at high temperatures (data not shown).

3.2. AFM observations of LB transferred films

To examine the PcSn10/DPPC films, and in particular the elliptical-shaped domains previously observed with BAM, the films were LB transferred on mica to be studied with AFM. All AFM observations were made at high vacuum. Most of the AFM observations that will be presented correspond to films with a concentration of $X_{PcSn10} = 0.87$, which were developed at pH = 5.6–5.8 and transferred at 4 mN/m. In Fig. 7, we present topographic images of the phase separation domains with an elliptical shape, similar to those observed with BAM in the film at the air/water interface, when the scales of observation are similar. However, these domains present some structure inside them that could not be observed in BAM images, when the LB films are observed at a higher resolution with AFM. We observe inside the elliptical-shaped domains many highlands and grooves, as well as peaks that are not homogeneously distributed along the rim of the domain. The bottom of the groves is approximately at the same level as the film that is outside the elliptical-shaped domains, and the highlands can be several nanometers above that level ($\sim$9–15 nm). These images reveal that the phase separation domains are formed by multilayers taking into account the DPPC and PcSn10 sizes (Fig. 1). These multilayers should be disposed in some regular molecular order to give rise the optical activity observed with the BAM images. Outside the elliptical-shaped domains, we find a homogeneous flat surface. This flat surface also cannot be a monolayer, because even at concentrations where elliptical-shaped domains do not appear ($0.55 \leqslant X_{PcSn10} \leqslant 0.70$) when the film is isothermally compressed, Π starts to increase at area densities less than 80 Å^2/molec, which correspond to an area much smaller than that occupied by all the PcSn10 and DPPC molecules at these concentrations. This is revealed by a simple calculation taking into account that for PcSn10, according to the sizes in Fig. 1, the collapse area density should be roughly around 196 Å^2/molec, when the PcSn10 molecules would be lying flat upon the air/water interface, or 176 Å^2/molec when they would be lying edge-on over the interface (averaging the vertical length). For the case of DPPC, its size is roughly given by the area density for collapse, which is close $\sim$43–45 Å^2/molec, as observed in its Langmuir isotherm (Fig. 2).

In Fig. 8, we present a topographic image using the DFM detection method. Very detailed images of the phase separation elliptical-shaped domains were obtained, as well as from the film outside them. In the example presented in Fig. 8, the domain forms an

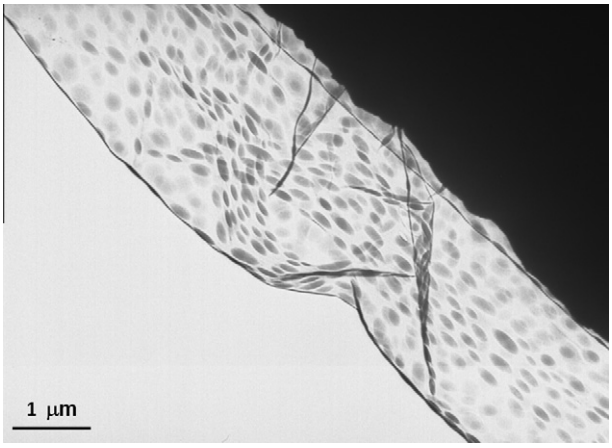

Fig. 9. Damaged collodion of a carbon-coated TEM grid, with a LB transferred film made of DPPC/PcSn10, as a result of its interaction with the transmission electron microscope beam. However, the image shows the presence of elliptical-shaped domains in the specimen.

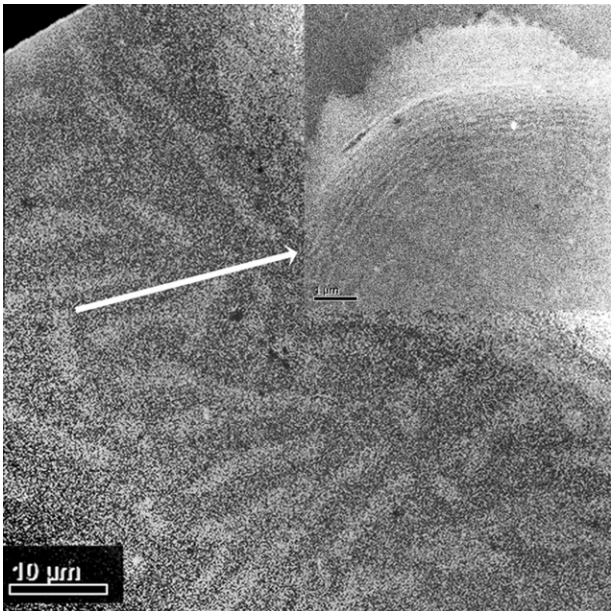

Fig. 10. HAADF TEM micrographs of a PcSn10/DPPC film, LB transferred onto a collodion-coated Cu TEM grid. Bright domains are enriched in the heavy metal (Sn) of PcSn10, and the dark background is depleted in this heavy metal. The inset presents a magnification around the edge of the elliptic domain indicated with the arrow.

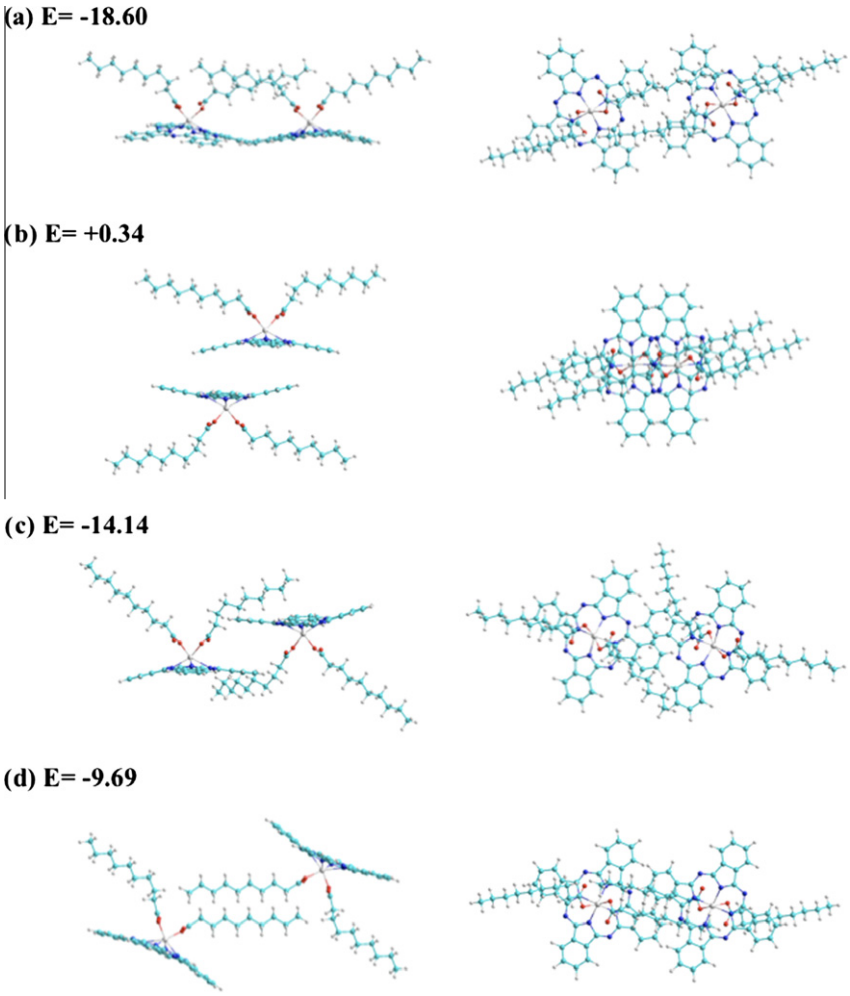

Fig. 11. Optimized chemical structures for the PcSn10–PcSn10 dimeric assemblies obtained with semiempirical calculations (PM3 method) and their corresponding energies. Lateral view (left side) and view from above (right side) for the dimeric assemblies: (a) Dim1; (b) Dim2; (c) Dim3; and (d) Dim4. The calculated energy of the dimeric assemblies is in kcal/mol.

elliptical plateau, which is decorated with both elongated holes and very small elongated bumps of the order of 100 nm (long axis) that are relatively aligned. The plateau height is ~1.6 nm above the external flat film. This height is roughly the size of PcSn10 molecule lying edge-on (Fig. 1b). The elongated holes and bumps can be observed in the medium and lower panels of Fig. 8a. Here, the heights are consistent with multilayers formed by one to three PcSn10 molecules laying edge on. Fig. 8b presents an image of the film outside the elliptical-shaped domain. It forms a homogeneous flat surface decorated with island-like structures of different heights, and many of them are elongated of with long axis ~200 nm and surely formed by several layers because their heights are larger than 10 nm. As before the AFM images, reveals heights consistent with a film made of multilayers.

3.3. Z contrast observations with HAADF

To get a rough estimate of the chemical composition of the elliptical-shaped domains in the DPPC/PcSn10 films, they were LB transferred onto collodion-coated Cu TEM grids, to be studied with HAADF TEM (true *Z*-contrast). First, conventional TEM mode was used on specimens, previously covered with a very small film of carbon, to make the film more resistant to the electron beam interaction. However, even with this protection, the collodion films with the LB transferred films were damaged when they interacted with the beam, as it is observed in Fig. 9. In spite of this problem, this image reveals the presence of elliptical-shaped domains in the observed specimen, which are similar to those observed with BAM at the air/water interface, and to those observed with AFM in the LB films transferred on mica. Therefore, films can be transferred onto the collodion of the TEM grids, although their lifetime under the electron beam is limited. It is important to note two features in this image: (1) the size of the domains does not correspond to those previously observed because the collodion is shrunk after being damaged and (2) the gray hue of the domains with respect to their surroundings reveals a larger relative concentration in a compound which scatters more electrons, as it could be a heavy metal, namely the tin atoms in the PcSn10 molecules. Fig. 10 shows a HAADF TEM micrograph with bright elliptical-shaped domains of the order of 10 μm on a darker homogeneous background. The bright areas are enriched in the heavy metal, Sn, contained in the PcSn10 molecule, and the dark areas are depleted in that heavy metal. Therefore, elliptical-shaped domains are enriched in PcSn10, and the film outside the domains has to be enriched in DPPC. The inset presents a magnification around the edge of the elliptic domain indicated with the arrow. Here, we observe that the distribution of the PcSn10 molecules is not homogeneous close to the rim of the elliptic-shaped domains. Apparently, they are formed by layered strips of slightly different composition in PcSn10 and DPPC, and this kind of structure fades away as we go inside the domains.

4. Semiempirical calculations of PcSn10 and of its dimeric assemblies

To get some clue about how PcSn10 molecules interact to self-assemble in films at the air/water interface, a computational study was carried out. This will be of help to develop a model for films with a very high concentration of PcSn10, or when the DPPC concentration is not able to perturb the PcSn10 organization. This is the case of films made of pure PcSn10, or of the elliptical-shaped domains that appears in films that are highly concentrated in PcSn10 (>98%); here, these domains have to be richer in PcSn10 than the nominal concentration value assigned to these films, thanks to the phase separation as evidenced by HAADF TEM experiments. In the computational survey, we determined how the PcSn10 molecules interact among themselves in vacuum. As a starting point to get the molecular geometry, the crystallographic coordinates of PcSn10 in the CSD were used to build monomeric species of PcSn10 (**Mon**) and of for four dimeric PcSn10–PcSn10 assemblies (**Dim**s). These four dimeric PcSn10–PcSn10 assemblies (**Dim1**, **Dim2**, **Dim3**, and **Dim4**) were initially constructed with the nearest crystalline neighbors. The PM3 method was used to optimize the chemical structures of the **Mon** and the **Dim**s species, and to get their interaction energy. The resulting equilibrium geometry for **Mon** is presented in Fig. 1b and for the four **Dim** pairs is presented in Fig. 11. A relative energetic stability trend was obtained from our calculations, when the four studied dimeric assemblies are compared with respect to a couple of molecules of PcSn10 at infinite separation ($2 \times$ **Mon**), which is taken as an energetic reference. The relative order of stability of the calculated dimers is: **Dim1** (-18.60) > **Dim3** (-14.14) > **Dim4** (-9.69) > $2 \times$ **Mon** (0) > **Dim2** (0.34); inside parenthesis, the calculated energy of the dimers with respect to the reference is in kcal/mol. The most stable dimeric assembly is **Dim1**, at least in the gas phase. Then, it is reasonable to suppose that **Dim1** is the most preferred dimeric assembly in a thin layer over the air/water interface, and **Dim2** would be the least preferred.

The relative stability energetic trend reveals the most probable form in which these dimeric assemblies can geometrically arrange to build a model film. This can be obtained by assembling PcSn10 molecules, all the way through repeating them to build a two-dimensional film using the dimeric assemblies **Dim1**, **Dim3**, and **Dim4**, along each direction of the crystallographic unit cell defined by these dimers, and avoiding type **Dim2**. In this way, a crystallographic layer was constructed just by repeating the **Dim 1** pairs in one direction, which defines vectors **a** and **b**, see Fig. 12. By repeating **Dim3** and **Dim4** pairs, we built the crystallographic layer in the other direction, defining vectors **b** and **c**, see Fig. 12. We ended up with a film that has actually two layers of PcSn10 disposed in very peculiar way that is presented in Fig. 13. Here, we can observe the crystal face defined by vectors **a** and **c**, as well as two tilted views to appreciate the organization of PcSn10 molecules. This face of the crystal is a good candidate of a model of the film at the air/water interface when the DPPC concentration is negligible. An important result obtained with this computational survey is that we can calculate the area of the ($|\mathbf{a} \times \mathbf{c}|$) = 196.72 Å^2 unit cell face using our calculated $\mathbf{a} = 13.2\ \mathbf{e_a}$ Å, $\mathbf{b} = 13.4\ \mathbf{e_b}$ Å, and $\mathbf{c} = 14.9\ \mathbf{e_c}$ Å. However, since within the unit cell, there are two PcSn10 molecules, the molecular area of PcSn10 in the crystal is ($|\mathbf{a} \times \mathbf{c}|$)/2 $\sim$ 98.36 Å^2. This value is very near to the value of $\sim$70–80 Å^2/molec obtained from the film collapse in the case of pure PcSn10. This area is also close to the area where Π is starting to increase in films which are very concentrated in PcSn10. As we can observe in Fig. 13, the molecular packing in the film seems to be quite dense; therefore, we would expect that this film would be very incompressible. This agrees with the high incompressibility observed in the case of film

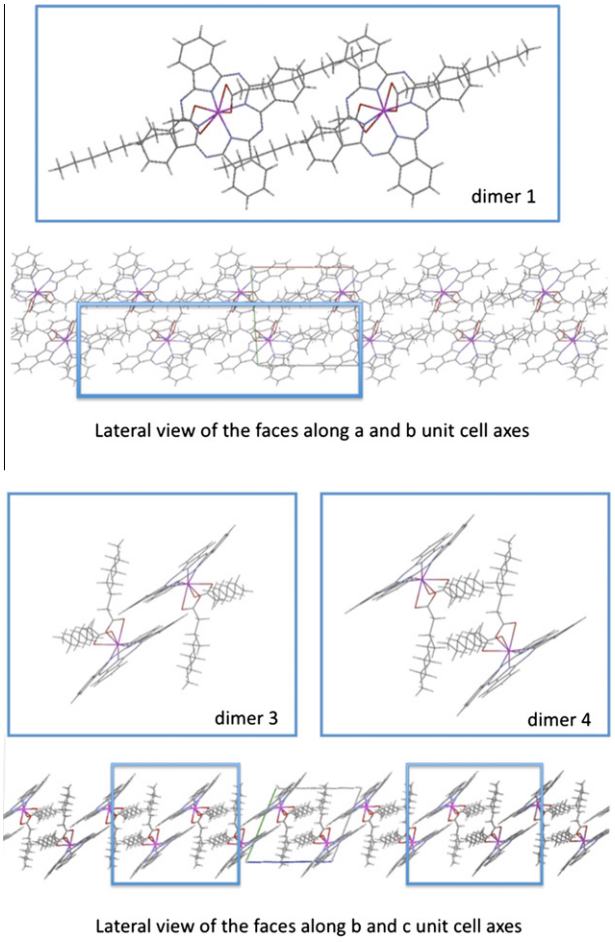

Fig. 12. Different views of PcSn10 dimers forming layers in a two-dimensional film defined by the packing crystallographic direction vectors **a** and **b**, and by **b** and **c**.

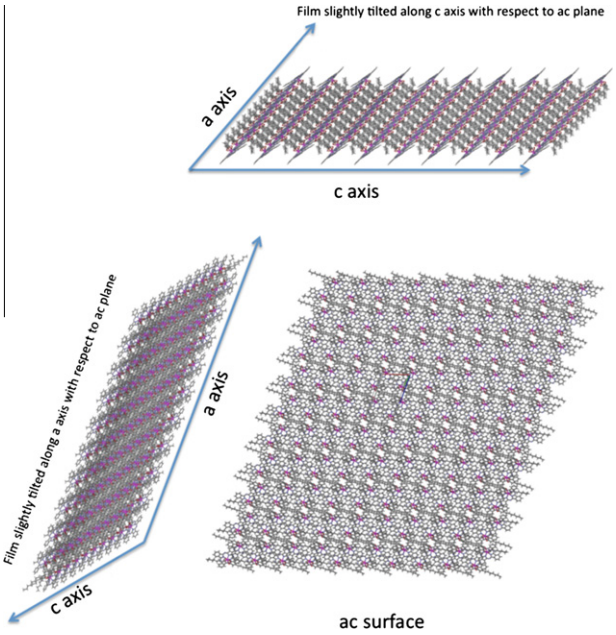

Fig. 13. Model for the film of PcSn10 when the DPPC concentration is very low. The crystal film was packed with the calculated energetic restrictions described in the text.

made of pure PcSn10, which seems typical of a crystalline film. However, it is not clear how the DPPC would interact with this compact film and to modify so critically its behavior as shown in the present work. Clearly, more research is needed to fully understand this issue. This model is not realistic when DPPC is present, since the interaction of DPPC with PcSn10 is really strong, even small quantities of DPPC in the film (∼1–2%) modify it, in an important way.

5. Concluding remarks

Compression isotherms and BAM observations of films made of PcSn10 and DPPC deposited on the air/water interface were presented. At $X_{PcSn10} \leqslant 0.70$, BAM observations reveal a homogeneous film that most of the times shows just one kind of shade, and there are no domains revealing segregation or some kind of molecular order, which could give origin to different textures.

In films rich in PcSn10 ($X_{PcSn10} > 0.70$), elliptical-shaped domains reminiscent of a phase separation were observed at the air/water (pH ∼ 5.8) interface, which have a different hue of gray depending on their orientation with respect to polarized light, revealing that the domains present optical anisotropy, surely as a consequence of a specific molecular order. LB transferred films on collodion-coated Cu grids revealed by using HAADF that the elliptical-shaped domains are enriched in PcSn10, and the film outside them is enriched in DPPC. Area/molecule in the isotherms close to film collapse and AFM measurements of LB films transferred on mica indicate that the film is actually made of multilayers. For pure PcSn10 films, a computational survey was performed using a PM3 method to determine how these molecules prefer to self-ensemble. The relative energetic stability for several dimeric assemblies was obtained, and a crystal model of the film was developed through packing and repeating PcSn10 molecules along the crystallographic directions, following the energetic order obtained between the different dimeric assemblies. From this study, it is clear that the interaction between DPPC and PcSn10 is really strong, even small quantities of DPPC in the film (∼1–2%) modify it in an important way. More research is needed to understand the PcSn10–DPPC interaction.

In relation to the motivation of this study, we would expect that in liposome preparation, homogeneous uniform films would be formed in the leaflets of the phospholipid liposome bilayers, when the added quantities of the phthalocyanine under study do not exceed a concentration of the order of $X_{PcSn10} \sim 0.70$. Although the phospholipid used here is an important component in actual liposome formulations, a next step to be done in the future would be to determine the effect of adding PcSn10 on the formation of actual liposomes; probably the elliptical-shaped domains obtained in films at high concentrations of PcSn10 would make them unstable. In addition, a suitable phospholipid mixture appropriate to fabricate bilayer or multilayer liposomes for the administration of the PcSn10, particularly at physiological conditions, has to be determined, as well as the PcSn10 concentration that those liposomes can support, and finally it is necessary to determine whether these vehicles could actually be used as a deliver system in cancer treatment with photodynamic therapy.

Acknowledgments

Funds from SEP-CONACYT (81081), DGAPA-UNAM (112508), UAM (11/2007), and TWAS (06-299 RG/PHYS/LA) are gratefully acknowledged. Also we thank to R. Hernandez for his assistance in TEM observations.

References

[1] N.B. McKeown, Phthalocyanine Materials: Synthesis, Structure, and Function, Cambridge University Press, 1998.
[2] C.C. Leznoff, A.B.P. Lever (Eds.), Phthalocyanines: Properties and Applications, vol. 1, VCH, New York, 1989, p. 436.
[3] N. Kobayashi, C.C.J. Leznoff, Porphyrins Phthalocyanines 8 (2004) 1015.
[4] S. Baker, M.C. Petty, G.G. Roberts, M.V. Twigg, Thin Solid Films 9 (1983) 53.
[5] W.R. Barger, A.W. Snow, H. Wohltjen, N.L. Jarvis, Thin Solid Films 13 (1985) 197.
[6] P. Smolenyak, R. Peterson, K. Nebesny, M. Torker, D.F. O'Brien, N.R.J. Armstrong, Am. Chem. Soc. 121 (1999) 8628.
[7] M.J. Cook, Pure Appl. Chem. 71 (1999) 2145.
[8] X.H. Qiu, C. Wang, Q.D. Zeng, B. Xu, S.X. Yin, H.N. Wang, S.D. Xu, C.L.J. Bai, Am. Chem. Soc. 122 (2000) 5550.
[9] M. Kimura, H. Ueki, K. Ohta, H. Shirai, N. Kobayashi, Langmuir 22 (2006) 5051.
[10] H. Benten, N. Kudo, H. Ohkita, S. Ito, Thin Solid Films 517 (2009) 2016.
[11] T.G. Gopakumar, M. Lackinger, M. Hackert, F. Muller, M.J. Hietschold, Phys. Chem. B 108 (2004) 7839.
[12] M. Lackinger, M. Hietschold, Surf. Sci 520 (2002) L619.
[13] Y. Wei, S.W. Robey, J.E. Reutt-Robey, J. Phys. Chem. C 112 (2008) 18537.
[14] N. Kilinc, D. Atilla, S. Ozturk, A.G. Gurek, Z.Z. Ozturk, V. Ahsen, Thin Solid Films 517 (2009) 6206.
[15] D.H. Gu, Q.Y. Chen, X.D. Tang, F.X. Gan, S.Y. Shen, K. Liu, H.J. Xu, Opt. Commun. 121 (1995) 125.
[16] S. Siebentritt, S. Gunster, D. Meissner, Synth. Met. 41 (1991) 1173.
[17] M.M. Ayhan, M. Durmus, A.G.J. Gurek, Porphyrins Phthalocyanines 13 (2009) 722.
[18] S.A. Priola, A. Raines, W.S. Caughey, Science 287 (2000) 1503.
[19] K. Ishii, M. Shiine, Y. Shimizu, S.I. Hoshino, H. Abe, K. Sogawa, N. Kobayashi, J. Phys. Chem. B 112 (2008) 3138.
[20] M.E. Rodriguez, P. Zhang, K. Azizuddin, G.B. De los Santos, S.M. Chiu, L.Y. Xue, J.C. Berlin, X.Z. Peng, H.Q. Wu, M. Lam, A.L. Nieminen, M.E. Kenney, N.L. Oleinick, Photochem. Photobiol. 85 (2009) 1189.
[21] P.A. Barbugli, M.P. Siqueira-Moura, E.M. Espreafico, A.C. Tedesco, J. Nanosci. Nanotechnol. 10 (2010) 569.
[22] H.I. Beltran, R. Esquivel, A. Sosa-Sanchez, J.L. Sosa-Sanchez, H. Hopfl, V. Barba, N. Farfan, M.G. Garcia, O. Olivares-Xometl, L.S. Zamudio-Rivera, Inorg. Chem. 43 (2004) 3555.
[23] H.I. Beltran, R. Esquivel, M. Lozada-Cassou, M.A. Dominguez-Aguilar, A. Sosa-Sanchez, J.L. Sosa-Sanchez, H. Hopfl, V. Barba, R. Luna-Garcia, N. Farfan, L.S. Zamudio-Rivera, Chem. Eur. J. 11 (2005) 2705.
[24] D. Hoenig, D.J. Moebius, Phys. Chem. 95 (1991) 4590.
[25] S. Henon, J. Meunier, Rev. Sci. Instrum. 62 (1991) 936.
[26] F.J. Giessibl, Rev. Mod. Phys. 75 (2003) 949.
[27] T. Albrecht, P. Grütter, D. Horne, D. Rugar, J. Appl. Phys. 69 (1991) 68.
[28] S. Utsunomiya, R.C. Ewing, Environ. Sci. Technol. 37 (2003) 786.
[29] J. Loos, E. Sourty, K. Lu, G. de With, S.V. Bavel, Macromolecules 42 (2009) 2581.
[30] HyperChem, HyperChem AC Release 8.0; 8.0 ed., Hypercube, Inc., 1115 NW 4th Street: Gainesville, Florida 32601, USA, 2007.
[31] J.J.P.J. Stewart, Comput. Chem. 10 (1989) 209.
[32] J.J.P.J. Stewart, Comput. Chem. 10 (1989) 221.
[33] E.M. Mitchell, F.H. Allen, O. Kennard, Chem. Inf. Syst. (1990) 63.
[34] F.H. Allen, J.E. Davies, J.J. Galloy, O. Johnson, O. Kennard, C.F. Macrae, E.M. Mitchell, G.F. Mitchell, J.M. Smith, D.G.J. Watson, Chem. Inf. Comput. Sci. 31 (1991) 187.
[35] M.J. Stilman, T. Nyokong, in: C.C. Leznoff, A.B.P. Lever (Eds.), Phthalocyanines: Properties and Applications, vol. 1, VCH, New York, 1989, p. 135.
[36] V.M. Kaganer, H. Möhwald, P. Dutta, Rev. Mod. Phys. 71 (1999) 779.
[37] N. Krasteva, D. Vollhardt, G. Brezesinski, H. Möhwald, Langmuir 17 (2001) 1209.
[38] W.R. Schief, S.G. Hall, V. Vogel, Phys. Rev. E 62 (2000) 6831.
[39] A.E. Wiacek, Colloids Surf. A: Physicochem. Eng. Aspects 302 (2007) 141.